44th AIAA Plasmadynamics and Lasers Conference
24-27 June 2013, San Diego, CA
AIAA-2013-3133

The Effects of Wall Cooling on Aero-Optical Aberrations Caused by Subsonic Turbulent Boundary Layers

Adam E. Smith[1] and Stanislav Gordeyev[2]
University of Notre Dame, Notre Dame, Indiana, 46556

Results of recent experimental measurements of the effect of partial wall cooling on aero-optical aberrations in subsonic, compressible turbulent boundary layers are presented for a range of subsonic Mach numbers and partial wall cooling locations. Optical measurements with high spatial- and temporal-resolution are obtained with a Malley Probe for a range of wall temperatures and for different cooling section lengths and locations. Detailed statistical analysis of temporal spectra and average values of aero-optical distortions are presented as a function of wall temperature to evaluate the effect of modified wall temperature on optical wavefront fluctuations and boundary layer turbulent structures. It was concluded that the near-aperture wall cooling is more efficient way to reduce aero-optical distortions, compared to the far-upstream wall cooling. In addition, modifications to the theoretical model which predicts levels of aero-optic aberrations for partial wall cooling are presented and discussed.

I. Introduction

IN the region immediately around an aerodynamic vehicle, the presence of turbulent density fluctuations can alter the local speed of light passing into and/or out of the aircraft through the turbulent region. This physical phenomenon, known as the aero-optic problem, is a consequence of the relationship between index-of-refraction, n, and density in air, ρ, via the Gladstone-Dale constant, K_{GD} (which is approximately 2.27×10^{-4} m^3/kg in air for visible wavelengths of light),

$$n(\vec{x},t)-1=K_{GD}\rho(\vec{x},t). \tag{1}$$

Light passing through regions of unsteady turbulent aerodynamic flow is unsteadily distorted by the spatially- and temporally-fluctuating density fields present along the optical path length. This might pose a significant problem for the performance of airborne optical system, whether they are directed energy, imaging, or free-space communications applications, as small disturbances to optical wavefronts in the near-field can result in significant reductions in time-average and instantaneous on-target intensity at points very far away from the aircraft [1,2].

As planar wavefronts propagate through these unsteady density distributions, the effect of turbulent density fluctuations on the propagation of light can be quantified by defining the Optical Path Length (OPL) as the integral of the index-of-refraction of a medium along the physical length traversed by a ray of light. It follows from equation (1) then that OPL can be expressed as

$$\mathrm{OPL}(x,y,t)=\int_a^b n(x,y,z,t)dz=\int_a^b\left[K_{GD}\rho(x,y,z,t)+1\right]dz, \tag{2}$$

where z is the direction of beam propagation. The resulting deviation from the average OPL can then be expressed as the Optical Path Difference (OPD),

$$\mathrm{OPD}(\vec{x},t)=\mathrm{OPL}(\vec{x},t)-\overline{\mathrm{OPL}(\vec{x},t)}, \tag{3}$$

where the overbar denotes spatial averaging. It can be shown that OPD is in fact the conjugate of the zero-mean wavefront, $W(\vec{x},t)=-\mathrm{OPD}(\vec{x},t)$.

The earliest investigations of the effects of compressible, turbulent flow on the propagation of light were performed by H.W. Liepmann, who in 1952 measured the angular jitter of a narrow beam of light as it passed through compressible, turbulent boundary layers (TBL) on the side walls of high-speed wind tunnels in order to characterize the sharpness of Schlieren photographs obtained in the facility [3]. Further experimental work on the diffusion of light by boundary layers done by Stine & Winovich [4] indicated that the radiant power scattered is

[1] Graduate Student, Department of Mechanical and Aerospace Engineering, Hessert Laboratory for Aerospace Research, Notre Dame, IN 46556, Student Member.
[2] Research Associate Professor, Department of Mechanical and Aerospace Engineering, Hessert Laboratory for Aerospace Research, Notre Dame, IN 46556, Senior AIAA Member.

dependent on both the integral length scale and intensity of density fluctuations within the turbulent boundary layer. As a result of the good agreement between levels of optical scattering and the characteristics of the turbulent density structure, the potential for inferring turbulent scales from measurements of optical aberrations was discussed [4]. In the late 1960's, Sutton [5] introduced the most widely-referred to theoretical formulation for the aberrating effects of turbulent boundary layers based on turbulence statistics, using an approach which was based heavily on Tatarski's [6] treatment of electromagnetic waves propagated through the atmosphere. The resulting 'linking equation' relating turbulence quantities and levels of optical distortions is given as

$$\mathrm{OPD}_{rms}^2 = 2K_{GD}^2 \int_0^L \rho_{rms}^2 \Lambda(y) dy \,, \tag{4}$$

where OPD_{rms} is the root-mean-square of the OPD, $\rho_{rms}(y)$ is the root-mean-square density fluctuation profile along the beam direction, and $\Lambda(y)$ is the density correlation length [5]. Jumper and Fitzgerald [1] showed that Sutton's 'linking equation' result is equivalent to the formulation put forth by Liepmann [3] by utilizing the assumption from Malley, et al. [7] that as turbulent structures and their corresponding wavefront aberrations convect at the same velocity. Recent CFD studies of the aero-optics of TBL by Wang & Wang where wavefront aberrations were computed by integrating through the computed density field have also shown good agreement with predictions from the linking equation [8].

In the 1990's, as flight test programs for airborne optical systems shifted from mid/far-infrared wavelength lasers ($\lambda \approx 10$ μm) to near-infrared wavelengths in the neighborhood of 1 μm in order to increase the systems' diffraction limited range, the problems posed by aero-optically active turbulent flow surrounding an aircraft became exacerbated due to the relationship between the ratio of diffraction limited far-field intensity, or Strehl ratio *SR*, and the wavefront error as defined by the Large-Aperture approximation;

$$SR = e^{-(2\pi \mathrm{OPD}_{rms}/\lambda)^2} \,. \tag{5}$$

This meant that while an aero-optic aberration with $\mathrm{OPD}_{rms} = 0.1$ μm would have resulted in a Strehl ratio around 99% for a laser wavelength of approximately 10 μm, when a 1 μm wavelength beam is passed through that same aberration the resultant Strehl ratio is reduced to just over 67% [1]. For this reason, research on the aero-optic effects of the turbulent boundary layer continued into the late 1990s and 2000s with a focus on developing robust predictive models for levels of optical aberrations, and on understanding the physical processes responsible for the greater part of optical aberrations so that methods of flow-control for aero-optic mitigation could be identified and tested [1].

A critical advancement in the aero-optic characterization of the turbulent boundary layer, and other aero-optically active flows, was the introduction of high-bandwidth wavefront sensing devices which allow for not only time-average measurements of levels of OPD_{rms}, but also time resolved measurements of wavefront aberrations. Malley, et al. [7] was the first to introduce a wavefront sensor capable of time-resolved measurements by measuring the angle at which a small-aperture beam was deflected by turbulent flow as a function of time; $\theta(t)$. Using the assumption that wavefront aberrations and turbulent structures convect together at some convection velocity U_C, a 1-D streamwise 'slice' of OPD could be reconstructed by first computing the OPL by the integral

$$\mathrm{OPL}(t) = -U_C \int_0^t \theta(\tau) d\tau, \tag{6}$$

where τ is a placeholder for time. OPD is then computed using equation (3).

In 2009, Wyckham & Smits pioneered the use of a high-speed camera and a lenslet array to create a high-bandwidth Shack-Hartmann wavefront sensor, which allowed for measurements of aero-optic aberrations with good spatial and temporal resolution [9]. Recent careful comparisons of 1-D high-bandwidth wavefront measurements made with the Malley probe, and spatially and temporally resolved wavefront measurements made with the high-speed Shack-Hartmann wavefront sensor have shown good agreement for turbulent boundary layers in the transonic (M_∞ = 0.4..0.7) regime, validating the accuracy of the underlying assumptions of the Malley probe wavefront reconstruction for TBL measurements [10].

Time-resolved wavefront measurements of the turbulent boundary layer were obtained for the first time in 2003 by Gordeyev, et al. using the Malley probe, and the results demonstrated that $\mathrm{OPD}_{rms} \sim \rho\delta M^2$ for subsonic freestream velocities, where δ is the boundary layer thickness [11]. In further experimental work by Wittich, et al. [12], and Cress, et al. [13], the authors utilized spectral analysis of wavefront statistics in order to address signal-to-noise problems in Malley probe measurements. Using their improved analysis techniques, the statistical scaling of OPD_{rms} for subsonic, compressible turbulent boundary layers in the wall normal direction was found to be

$$\mathrm{OPD}_{rms} = A \frac{\rho_\infty}{\rho_{SL}} \delta^* M_\infty^2, \tag{7}$$

where δ^* is the boundary layer displacement thickness, and the empirical constant of proportionality $A = (1.7\pm0.2)\times10^{-5}$. The authors also found that measurements of convective velocity of aero-optical structures in TBL were approximately $0.82U_\infty$. This finding, in conjunction with observations that the spectral peak for Malley probe wavefront measurements are located around $St_\delta = 1$, suggests that the most optically active structures reside in the outer region of the turbulent boundary layer. These experimental findings have been supported by recent computational investigations of the aero-optics of boundary layers by Wang & Wang [8]. Based on aero-optical measurements for a supersonic boundary layer at $M = 2.0$, the statistical scaling was generalized for supersonic Mach numbers [14]. Additional experimental and modeling work has been performed by Cress, et al. [13,15] in characterizing the aero-optic effects of turbulent boundary layers as a function of additional parameters, including the angle of beam incidence, β, and the wall temperature, T_w; scaling relationships were developed and shown to be consistent with experimental data. White & Visbal have also performed Large Eddy Simulations aero-optic aberrations caused by compressible TBL. Computational results for different angles of beam incidence were shown to be in good agreement with experimental results obtained by Cress in [16]. Simulations performed for heated and cooled walls, however, have not been shown to be in good agreement with the theoretical model proposed in [15], and it was suggested that the reason for this is the breakdown of the underlying assumptions of this model at the lower Reynolds numbers at which the simulations were performed [17].

Recently, interest in reducing time average and instantaneous levels of aero-optic aberrations caused by turbulent boundary layers (TBL) for the purpose of free-space communications applications [18] has motivated research which seeks to identify and experimentally evaluate potential passive flow control techniques. Prior inferences from convective velocity and deflection angle spectra measurements that the most aero-optically active structures reside in the outer portion of the TBL led Smith & Gordeyev [19] to investigate the effects of Large-Eddy Breakup Devices (LEBUs), which act to break up large-scale turbulent structures in the outer portion of the TBL. The single-element LEBU devices tested were shown to locally reduce OPD_{rms} by up to 30% in the region up to 6δ downstream of the LEBU trailing edge. As a result, further TBL experiments on a wider class of passive outer-layer manipulators (including single- and multi-element LEBU devices, pin fences, screens, and honeycombs) have been proposed [19].

TBL wall-cooling was identified as another potential method for aero-optic mitigation by Cress [15]. The statistical model developed for wall temperature effects in [15] on aero-optic wavefront aberrations predicted that there is an optimal temperature which results in a reduction of about 80% in OPD_{rms}. While valuable preliminary measurements of OPD_{rms} in the wall-cooling regime were presented by Cress in [15], there is a need to obtain a wide range of points to validate the statistical model predictions in this regime.

In practical applications where this is of potential use, however, the energy expense of cooling of the full TBL development length in an airborne application might be impractical and/or cost-expensive, since freestream temperatures at several kilometers in altitude may be on the order of -50°C [15]. Therefore, it is of interest to investigate the effects of cooling only partial lengths of the boundary layer development section upstream of the optical aperture in order to investigate the levels of aero-optic mitigation that can be achieved while reducing the energy consumption of wall cooling mitigation techniques.

In this paper, the authors conducted a systematic investigation of wall-cooling and its effects on aero-optical distortions using the Malley probe 1-D wavefront sensor in order to fill the gap in experimental data for which would determine the validity of the theory proposed in [15]. Investigation of a number of partial-wall cooling cases was also performed in order to determine the effectiveness of partial wall-cooling for mitigation of TBL wavefront aberrations. An overview of the derivation of the statistical model developed by Cress [15] for the relationship between wall temperature and levels of aero-optic aberrations is given in Section II. The experimental facilities, test section configurations and measurement techniques are described in detail in Section III, and the resulting levels of wavefront aberrations are presented and compared to the statistical model in Section IV.

II. Statistical Model for Wall-Temperature Effects

The statistical model developed by Cress in [15] relating levels of OPD_{rms} in turbulent boundary layers with different wall temperatures is rooted in the large body of research which exists for heat transfer in boundary layers. The Strong Reynolds Analogy (SRA), presented by Morkovin in 1962, was an important advancement in this area of study, because it assumes that pressure fluctuations, p', in the turbulent boundary layer are negligible. This allows for a relationship between fluctuations in static temperature, T', and velocity fluctuations, u', to be formed from the Reynolds-averaged form of the boundary layer momentum and energy equations,

$$\frac{T'}{\overline{T}} = -(\gamma - 1)M^2 \frac{u'}{\overline{U}}, \tag{8}$$

where $\overline{T}$ and $\overline{U}$ are the average static temperature and velocity, respectively, γ is the specific heat ratio, and M is Mach number [15].

The SRA, however, neglects total temperature fluctuations in the turbulent boundary layer, and thus it is not sufficient to handle turbulent boundary layer heat transfer problems with non-adiabatic wall conditions. To overcome this limitation, Walz and van Driest introduced a relationship between temperature and velocity fluctuations where total temperature fluctuations are not neglected [15],

$$\frac{T}{T_\infty} = \frac{T_w}{T_\infty} + \frac{T_{aw} - T_w}{T_\infty}\left(\frac{u}{U_\infty}\right) - r\left(\frac{\gamma-1}{2}\right)M_\infty^2\left(\frac{u}{U_\infty}\right)^2, \tag{9a}$$

$$\frac{T''}{T_\infty} = -\frac{T_{aw} - T_w}{T_\infty}\left(\frac{u''}{U_\infty}\right) - r\left(\frac{Uu''}{c_p T_\infty}\right), \tag{9b}$$

where the recovery factor r is defined as $r = (T_{aw} - T_\infty)/(T_{o,\infty} - T_\infty)$. T_∞, and $T_{o,\infty}$, are the freestream static and total temperatures, respectively, T_w is the wall temperature, T_{aw} is the adiabatic wall temperature, c_p is the specific heat, u is the local streamwise velocity component, and U_∞ is the freestream velocity. This equation is known as the Walz equation, or the modified Crocco relation [15]. Replacing the fluctuating temperature and velocity terms in these equations with the root-mean-square of the temperature and velocity, T_{rms} and u_{rms} respectively, the following expression for T_{rms} is obtained [15],

$$\left(\frac{T_{rms}}{T_\infty}\right)^2 = \left(\frac{u_{rms}}{U_\infty}\right)^2 \times \left[\left(\frac{\Delta T}{T_\infty}\right)^2 + 2r(\gamma-1)M_\infty^2\frac{\Delta T}{T_\infty}\frac{u}{U_\infty} + \left(r(\gamma-1)M_\infty^2\frac{u}{U_\infty}\right)^2\right] \tag{10}$$

where $\Delta T = T_w - T_{aw}$, the difference between wall temperature T_w and the adiabatic wall temperature. It follows from the ideal gas law, $p = \rho RT$, that if p' is negligible, as the SRA assumes it to be, the root-mean-square of density fluctuations in the turbulent boundary layer can also be expressed in terms of T_{rms},

$$\left(\frac{\rho_{rms}}{\rho_\infty}\right)^2 = \left(\frac{T_{rms}}{T_\infty}\right)^2 \tag{11}$$

By combining (10) and (11) to obtain an expression for density fluctuations in the TBL and substituting this expression into the form of Sutton's linking equation shown in (4), Cress [15] derived the following expression for levels of OPD_{rms} caused by TBL with heat transfer, as a function of the wall temperature,

$$\mathrm{OPD}_{rms} = B_0\frac{\rho_\infty}{\rho_{SL}}\delta^*\left[B_1M^4 + B_2\left(\frac{\Delta T}{T_\infty}\right)M^2 + B_3\left(\frac{\Delta T}{T_\infty}\right)^2\right]^{1/2}. \tag{12a}$$

where y is the wall normal coordinate, and

$$\begin{aligned}
B_0 &= \sqrt{2}K_{GD}\rho_{SL}(\gamma-1),\\
B_1 &= \int_0^\infty\left[r^2\left(\frac{u(y)u_{rms}(y)}{U_\infty^2}\right)^2\frac{\Lambda(y)}{\delta^*}\right]d\left(\frac{y}{\delta^*}\right),\\
B_2 &= \int_0^\infty\left[\frac{2r}{(\gamma-1)}\frac{u(y)}{U_\infty}\left(\frac{u_{rms}(y)}{U_\infty^2}\right)^2\frac{\Lambda(y)}{\delta^*}\right]d\left(\frac{y}{\delta^*}\right),\\
B_3 &= \int_0^\infty\left[\left(\frac{u_{rms}(y)}{U_\infty(\gamma-1)}\right)^2\frac{\Lambda(y)}{\delta^*}\right]d\left(\frac{y}{\delta^*}\right).
\end{aligned} \tag{12b}$$

Several different functions for the wall-normal correlation lengths, shown in Figure 1, have been used in previous studies of aero-optic linking equation models of TBLs. The density correlation function Λ_1 is provided by Gilbert [20] and Λ_2 was measured by Rose and Johnson [21]. Wang & Wang [8] computed $\Lambda_3(y)$ from DNS results for a TBL at $Re_\theta = 3550$, which is order of magnitude smaller than the Reynolds number of the boundary layer in the present study.

The three functions used in this study are shown in Figure 1. If (12a) is simplified further by modifying the equation constants to that $A = B_0B_1^{1/2}$, $C_1 = B_2/B_1$, and $C_2 = B_3/B_1$, the statistical model reduces to

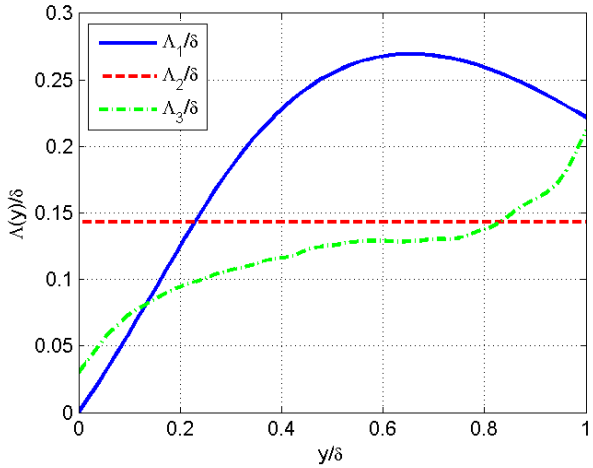

Figure 1. Density correlation length functions; Λ_1 presented by Gilbert (1982), Λ_2 measured by Rose & Johnson (1982), and Λ_3 computed from DNS of a Re_θ = 3550 TBL by Wang & Wang (2012).

$$\mathrm{OPD}_{rms} = A\frac{\rho_\infty}{\rho_{SL}}\delta^*\left[M^4 + C_1\left(\frac{\Delta T}{T_\infty}\right)M^2 + C_2\left(\frac{\Delta T}{T_\infty}\right)^2\right]^{1/2}. \tag{13}$$

Note that for ΔT = 0, (13) is reduced to be $\mathrm{OPD}_{rms} = A(\rho_\infty/\rho_{SL})\delta^* M^2$, which was shown to be a correct scaling for adiabatic subsonic Mach numbers below 0.8, although for higher Mach numbers it overestimates the level of aero-optical distortions [14].

Cress [15] reported that for velocity measurements in a M = 0.5 TBL, C_1 and C_2 were found to be 6.38 and 10.28, respectively. In addition, linearized form of equation (13) was found to work well for modeling wavefront measurements for wall-heating,

$$\mathrm{OPD}_{rms} = A\frac{\rho_\infty}{\rho_{SL}}\delta^*\left[M^2 + D_1\left(\frac{\Delta T}{T_\infty}\right)\right] \tag{14}$$

where the empirical constant $D_1 = C_1/2$ [15].

For the case where ΔT is negative, however, the linearized form of the model is not valid, as the parabolic form of the temperature terms in equation 11 indicates that there is some optimal value of wall cooling which results in a global minimum of OPD_{rms}. Taking the derivative of (13) with respect to ΔT, we obtain the expression for the optimal value of ΔT which gives the largest reduction in OPD_{rms};

$$\frac{\Delta T_{Optimal}}{T_\infty} = -\frac{1}{2}\left(\frac{C_1}{C_2}\right)M^2 \tag{15}$$

Equation (15) is only a function of Mach number M and the empirical constants C_1 and C_2. Using the values presented by Cress [15] for experimental measurements of velocity at M = 0.5, Figure 2 (left) shows predicted levels of OPD_{rms} from (13) as a function of wall temperature for several Mach numbers. This theoretical model predicts a reduction in OPD_{rms} of about 80% at the optimal wall cooling temperatures shown in Figure 2. The optimal wall-cooling temperature, $\Delta T_{Optimal}$, calculated from (15) as a function of freestream Mach number is also shown in Figure 2 (right). Since $\Delta T_{Optimal} \sim M^2$, it is of interest to investigate the effects of cooling finite portions of the wall upstream of the optical aperture, since partial wall cooling could be used to reduce the energy cost of this aero-optic mitigation technique.

Careful examination of equation (10) highlights that inherent in the derivation of this model is the assumption that the velocity structure in the TBL is not altered by the introduction of a non-adiabatic wall condition, but that the difference between adiabatic and actual wall temperatures ΔT acts as a scalar multiplier affecting the strength of the fluctuating temperature and density profiles in the TBL. This assumption was shown by Cress to be valid for modetare temparture differences, as deflection angle spectra for wall heating measurements exhibited self-similarity with wavefront measurements obtained at adiabatic wall temperatures when scaled using the statistical model for wall-temperatures. In this experiment, it is of interest to investigate whether spectra for a range of partial wall-cooling measurements and cold wall temperatures will also exhibit this self similarity, or whether partial wall

cooling will result in a well defined thermal sub-layer which will invalidate the assumptions made in the model derivation.

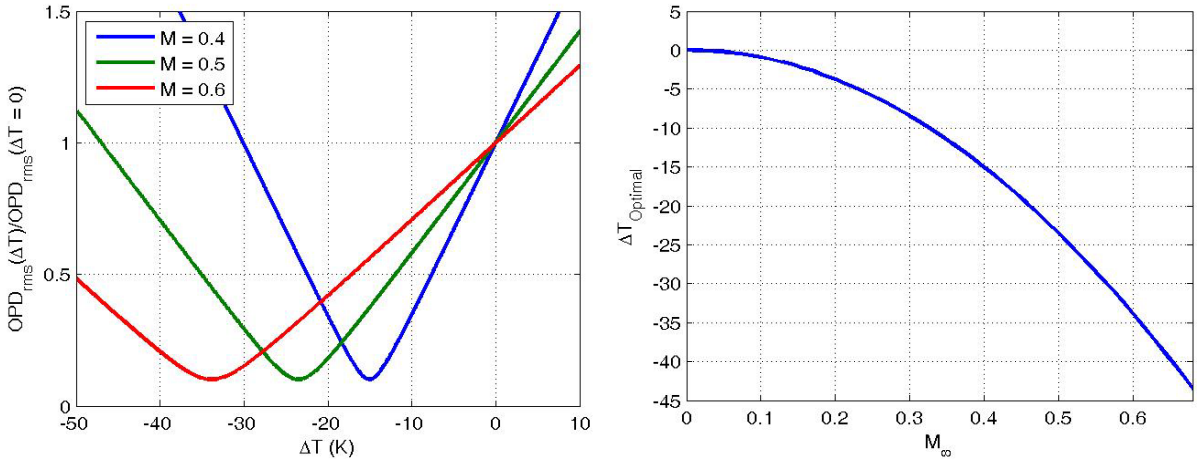

Figure 2. Predicted OPD_{rms} versus wall cooling temperature for different Mach numbers (left), and predicted optimal wall cooling temperatures (right) from (15), using C_1 and C_2 from [15].

III. Experimental Setup

Experimental measurements of wall cooling effects on the aero-optics of the turbulent boundary layer were conducted in the Transonic Wind Tunnel at the University of Notre Dame's Hessert Laboratory for Aerospace Research; a schematic of the experiment is shown in Figure 3. The wind tunnel has an open-loop design with an inlet contraction ratio of 150:1, followed by a Plexiglas boundary layer development section which has a cross section that measures 9.9 cm × 10.0 cm. The total length of the boundary layer development section is variable, and can be lengthened or shortened using 0.3 m modular sections to change the boundary layer thickness at the measurement section. In the current study, the total length to the beginning of the optical section is approximately 160 cm. In order to conduct boundary layer heat-transfer experiments, the upper wall of the test section was replaced with an 8 mm thick Aluminum plate from x = 0 cm to 150 cm. This configuration of the cooling wall test section is similar to the heated wall test section described in [15], which used an 8 mm thick Aluminum wall from x = 30 cm to x = 150 cm. Downstream of the boundary layer development section, portions of the Plexiglas on the upper and lower walls of the wind tunnel were replaced with optical quality glass plates in order to ensure accurate optical characterization of the boundary layer using aero-optic wavefront sensors. Static pressure ports on the side wall of

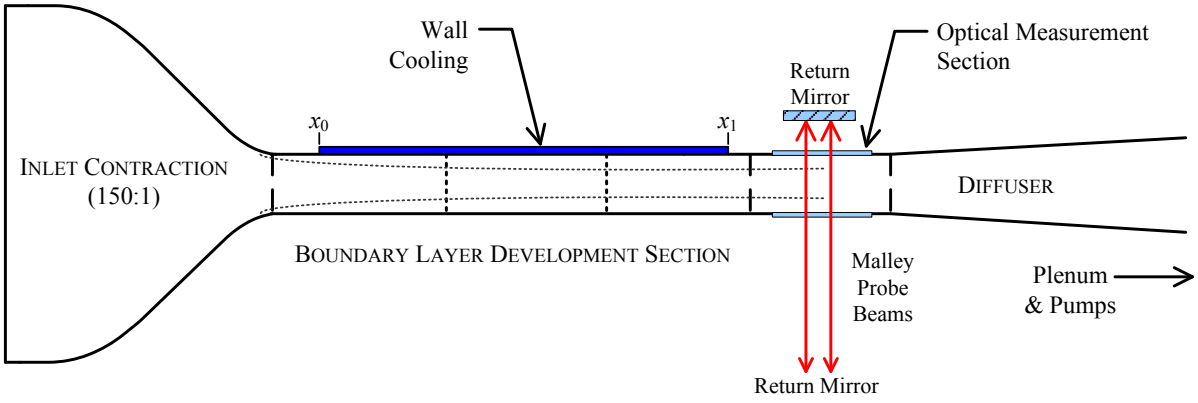

Figure 3. A schematic of the Hessert Transonic Wind Tunnel configured for aero-optic wavefront measurements of SBL wall-cooling flow control.

the optical measurement section were used to determine the free-stream velocity throughout the experiment. Previous experimental measurements in this facility [15] characterized the boundary layer profile using a hot-wire anemometer to obtain mean velocity, $u(y)$, and velocity RMS, $u_{rms}(y)$, profiles at a freestream mach number of M = 0.4. From these measurements the boundary layer thickness, δ, was found to be 2.4 cm and the displacement thickness, δ^*, was 3.15 mm.

To investigate the effects of full and partial wall cooling on levels of aero-optical aberrations, various lengths of the Aluminum plate on the upper wall of the boundary layer development section were cooled to a low temperature using dry ice while the wind tunnel was off, taking care to make sure the wall was uniformly cooled. Wall temperature was directly measured using thermocouples embedded in the aluminum plate at x = 22″, 36″, and 51″ in order to provide accurate wall temperature measurements over the length of the test section. After reaching a significantly low temperature (typically around −30°C), the dry ice was removed and the tunnel was switched on. Simultaneous wall-temperature, free-stream velocity, and wavefront measurements were then obtained as the tunnel wall temperature increased to the adiabatic wall temperature T_{aw}.

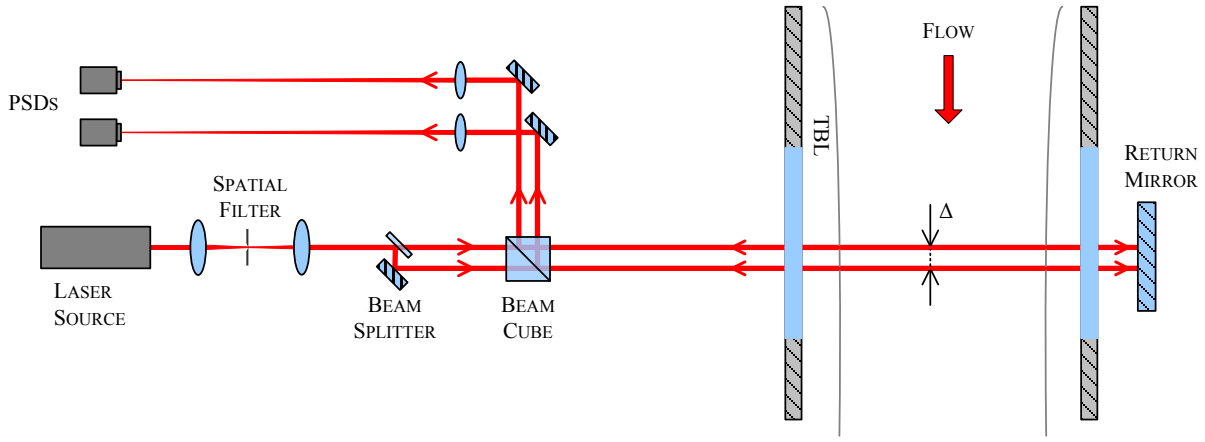

Figure 4. Schematic of the Malley Probe wavefront sensor.

One-dimensional wavefronts were acquired using the Malley Probe, the operation of which is described in detail by Gordeyev, et al [14], downstream of the cooling wall boundary layer development section at approximately x_{MP} = 162 cm. Using two beams aligned in the streamwise direction, as shown in Figure 4, each with a diameter of approximately 1 mm, time series of beam deflection angle $\theta(t)$ were sampled at 200 kHz for 10 seconds. From these time traces of the deflection angle, a number of quantities including deflection angle amplitude spectra, one-dimensional wavefronts, and OPD_{rms} can be computed using the frozen-flow assumption, $dx = U_c dt$, where the convective velocity U_c is computed from the phase delay between readings from two Malley beams aligned in the streamwise direction with separation Δ.

Assuming that the boundary layers on opposite side walls of the wind tunnel test section are statistically independent, the contribution of the wall-cooling modified boundary layer, OPD_{rms}^{SBL,T_w} may be isolated from the contribution of the un-modified boundary layer using an extension of the statistical relationship shown in [12,15],

$$OPD_{rms}^{SBL,T_w} = \sqrt{\left(OPD_{rms}^{DBL}\right)^2 + \tfrac{1}{2}\left(OPD_{rms}^{BASELINE}\right)^2},$$

where OPD_{rms}^{DBL} is the value of OPD_{rms} measured by a wavefront sensor passing through both the wall-cooling modified boundary layer and the un-modified boundary layer, and $OPD_{rms}^{BASELINE}$ is the value of OPD_{rms} measured by a wavefront sensor passing through two un-modified boundary layers in the control case. Similarly, it is also shown in [15] that deflection angle spectra of the LEBU-modified boundary layer can be extracted in a similar manner;

$$\hat{\theta}(f)_{SBL,T_w} = \sqrt{\left(\hat{\theta}(f)_{DBL}\right)^2 + \tfrac{1}{2}\left(\hat{\theta}(f)_{BASELINE}\right)^2}.$$

From the SBL scaled deflection angle spectra obtained for different wall temperatures, OPD_{rms} were computed using the Fourier-version of equation (6),

$$OPD_{rms}^2 = 2U_c^2 \int_0^\infty \left|\hat{\theta}(f)\right|^2 \Big/ (2\pi f)^2 \, df,$$

Table 1. Experimental configurations of the SBL wall-cooling wavefront measurements.

Case	x_0 (in.)	x_1 (in.)	L_{Cool} (in.)	R_{cool}
Near-Aperture 1	0.0	58.5	58.5	91.4%
Near-Aperture 2	12.0	58.5	46.5	72.6%
Near-Aperture 3	44.5	58.5	14.5	22.7%
Near-Aperture 4	31.0	58.5	27.5	43.0%
Near-Aperture 5	24.0	58.5	34.5	53.9%
Far-Upstream 1	12.0	27.0	15.0	23.4%
Far-Upstream 2	12.0	39.0	27.0	42.2%
Far-Upstream 3	12.0	46.0	34.0	53.1%

and plotted as a function of recovery temperature ΔT. For all cases, this method of computing OPD_{rms} allows for the exclusion of both low-frequency noise from tunnel vibration, and high-frequency noise peaks which are the result of RF and electronic noise sources present within the laboratory environment. To study the effects of partial wall-cooling wavefront measurements, two general categories of partial cooling were tested. The first category of test configurations is a set of near-aperture partial wall-cooling wavefront measurements, in which the cooling end location x_1 was fixed just upstream of the optical measurement section, and the cooling begin location x_0 was varied in order to change the length of cooling. The second category of partial wall-cooling tests was a set of wavefront measurements for far-upstream cooling, in which x_0 was fixed, and x_1 was varied in order to change the cooling length. A full list of the wall-cooling cases tested in this experiment is given in Table 1 along with the streamwise locations of the start, x_0, and end, x_1, of the cooled wall segments. The length of the boundary layer development section cooled, $L_{cool} = x_1 - x_0$, and the percentage of the boundary layer development length up to the Malley probe location, $R_{cool} = L_{cool}/x_{\mathrm{MP}}$, are given in Table 1 as well. In order to compare cooling wall results directly to results of wall heating in [15], the 'Near-Aperture 2' (73%) wall cooling case corresponds to the exact dimensions of wall heating experiments reported in [15]. Wavefront measurements were made with the Malley probe using the sampling conditions stated previously for all of the wall-cooling cases described in Table 1. Wavefronts were measured at freestream Mach numbers of 0.33, 0.4, and 0.5 for all wall cooling cases.

IV. Results & Analysis

From the 1-D Malley probe wavefront measurements obtained, SBL scaled deflection angle spectra were computed at a range of wall cooling temperatures for both full and partial wall cooling tests. Figure 5, left plot, shows a selected number of deflection angle spectra for the $M = 0.33$, full and partial wall-cooling case for varying wall cooling configurations and temperatures. Recalling the assumption from the derivation by Cress (2010) that non-adiabatic wall temperature acts as a scalar multiplier, and does not modify the structure of the turbulent boundary layer, it should follow that deflection angle spectra exhibit self-similarity when normalized by the levels of $\mathrm{OPD}_{rms}(\Delta T)$ from equation (13). A simplified version of (13) in which $\mathrm{OPD}_{rms}(\Delta T)$ is normalized by the level of OPD_{rms} measured for the baseline adiabatic wall temperature case, $\mathrm{OPD}_{rms}(T_{aw}) = A(\rho_\infty/\rho_{SL})\delta^* M^2$, is obtained by dividing equation (13) by $\mathrm{OPD}_{rms}(T_{aw})$,

$$\mathrm{OPD}_{rms}^{\mathrm{NORM}}(\Delta T) = \frac{\mathrm{OPD}_{rms}(\Delta T)}{\mathrm{OPD}_{rms}(T_{aw})} = \left[1 + C_1\left(\frac{\Delta T}{T_\infty}\frac{1}{M^2}\right) + C_2\left(\frac{\Delta T}{T_\infty}\frac{1}{M^2}\right)^2\right]^{1/2}. \tag{16}$$

This model now becomes purely a function of the empirical constants C_1 and C_2, and the non-dimensional term temperature-Mach number term $\Delta T/(T_\infty M^2)$. Therefore, data for the effect of wall cooling on OPD_{rms} at several different Mach numbers can be plotted in the non-dimensional form

$$\hat{\theta}_{NORM}(St_\delta) = \hat{\theta}(f) \Bigg/ \left(\frac{\rho_\infty}{\rho_{SL}}\delta^*\left[M^4 + C_1\left(\frac{\Delta T}{T_\infty}\right)M^2 + C_2\left(\frac{\Delta T}{T_\infty}\right)^2\right]^{1/2}\right), \tag{17}$$

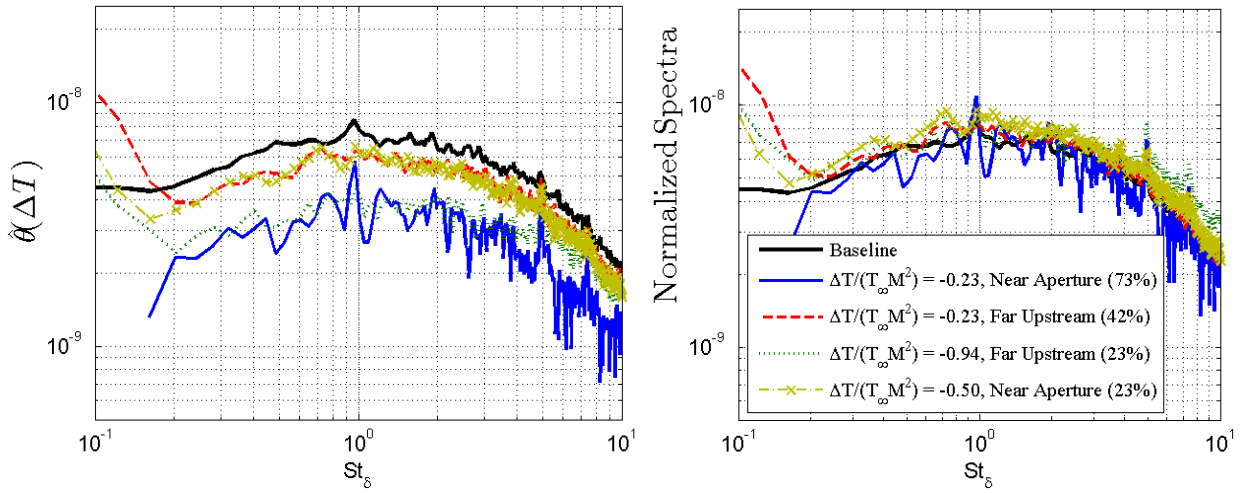

Figure 5. Deflection angle spectra (left), and normalized deflection angle spectra (right) for selected wall cooling configurations.

and the empirical constants can be estimated. Results of this normalization for the spectra shown in Figure 5, left plot, are presented in Figure 5, right plot. These normalized spectra demonstrate that these deflection angle spectra collapse reasonably well for both full and partial-wall cooling wavefront measurements.

Deflection angle spectra for several selected wall cooling cases, normalized by the baseline spectra, are plotted as a function of reduced frequency St_δ and a range of normalized wall temperatures $\Delta T/\left(T_\infty M^2\right)$ in Figure 6. Figure 6a) shows spectra for the near-aperture, R_{cool} = 73%, wall cooling case, which corresponds to the exact dimensions from [15]. For cooled wall temperatures, the normalized spectra surfaces show that the effect of non-adiabatic wall temperatures effects deflection angle spectra evenly across a wide band of frequencies. This result is consistent with the normalization shown in Figure 5 and for wall heating experiments in [15]. Spectra are plotted in the same manner for wall cooling cases where approximately half of the boundary layer development length was cooled in Figure 6b) and c). In both of these plots, low-frequency, $St_\delta < 1$, increases in the range $-0.8 > \Delta T/(T_\infty M^2) > -0.6$ corresponds to the effect of residual condensation from the cooling wall test section passing over the optical aperture. Normalized surface spectra for the near-aperture, R_{cool} = 54% in Figure 6b) shows broad-band reduction in deflection angle spectra similar to the effect observed for the 73% wall cooling case, although the strength of reduction in spectra is reduced compared to the longer wall cooling length. Figure 6c) shows a similar result for the far upstream, R_{cool} = 54% wall cooling case, although the reduced temperature at which the largest spectral reduction occurs is larger for the far upstream cooling case when compared to results from Figure 6b).

The effect of wall temperature on deflection angle spectra measured for short lengths (R_{cool} ~ 23%) lengths of wall cooling are plotted in Figure 6d) and e). For both near-aperture cooling in Figure 6d), and far upstream cooling shown in Figure 6e), wall cooling is also shown to results in broad-band reduction in deflection angle spectra up to at least $St_\delta \approx 5$. While spectra above $St_\delta = 5$ are not shown to be suppressed in the same way as spectra at lower frequencies, it has been shown previously that [22] that wavefront aberrations which correspond to $St_\delta > 5$ contribute less than 10% to total levels of optical aberrations. The presence of self-similarity and the broad-band reductions in deflection angle spectra for different partial wall cooling cases gives evidence that partial wall cooling does not significantly alter the turbulence structure of the boundary layer. Instead, partial wall cooling appears to act as a scalar multiplier for the level of density fluctuations predicted from velocity measurements, as is assumed in the development of the model equation (16). Therefore, it is reasonable to assume then that partial wall-cooling in the turbulent boundary layer may be modeled using equation (16), where empirical constants are modified as a function of the location and length of the wall-cooling region. Extending equation (16) for partial wall-cooling, assuming that the empirical constants C_1 and C_2 are functions of the start location, x_0, and end location x_1, of wall cooling,

$$\mathrm{OPD}_{rms}^{\mathrm{NORM}}\left(\Delta T\right)=\left[1+C_1\left(x_0,x_1\right)\left(\frac{\Delta T}{T_\infty}\frac{1}{M^2}\right)+C_2\left(x_0,x_1\right)\left(\frac{\Delta T}{T_\infty}\frac{1}{M^2}\right)^2\right]^{1/2}. \quad (18)$$

From experimental measurements, the values of C_1 and C_2 can be determined as a function of partial cooling parameters in order to explore the nature of this functional dependence.

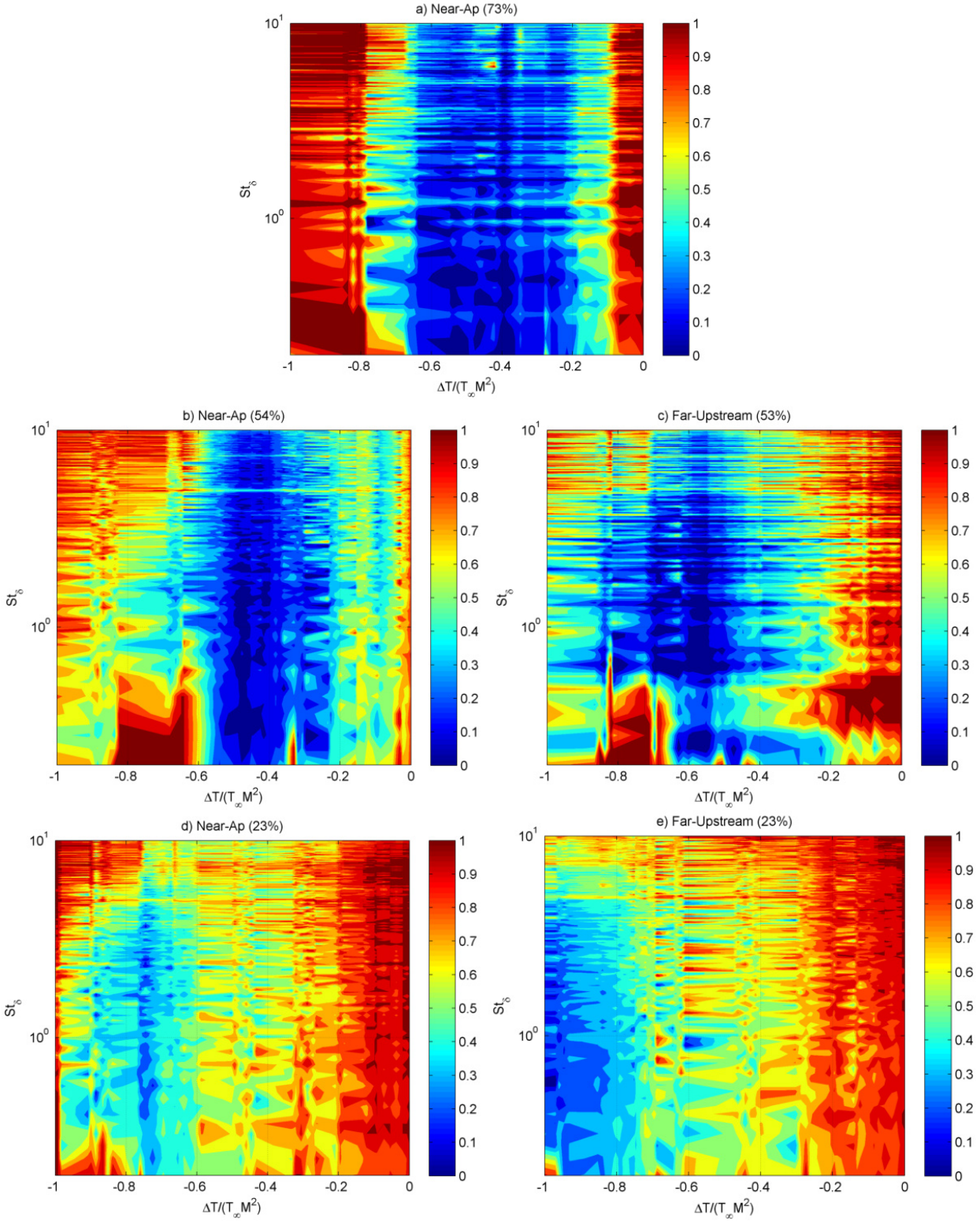

Figure 6. Baseline-normalized SBL spectra for a) near-aperture wall-cooling (R_{cool} = 73%), b) near-aperture cooling (54%), c) far-upstream cooling (53%), d) near-aperture cooling (23%), and e) far-upstream cooling (23%).

Measurements of $\mathrm{OPD}_{rms}^{\mathrm{NORM}}(\Delta T)$ for the 73% near-aperture cooling case are plotted in Figure 7 for all three Mach numbers at which wavefront measurements were obtained. Figure 6 shows $\mathrm{OPD}_{rms}^{\mathrm{NORM}}(\Delta T)$ as a function of absolute temperature difference ΔT. The data exhibits similarity to the behavior predicted by the theoretical equation (18) shown in Figure 7, right plot, with the location of the optimal cooling temperature decreasing as Mach number increases. In order to compare experimental results for all three Mach numbers to theory, OPD_{rms} measurements are re-plotted in Figure 7, right plot, as a function of the reduced temperature difference $\Delta T/(T_\infty M^2)$. Results of all three freestream velocities tested are in very good agreement with one another and with a fit of the theoretical model (18), where the constants, C_1 and C_2 were calculated to be approximately 4.167 and 4.630, respectively. Recall that for the linearized model from Cress [15], this result would correspond to a value of D_1 = 2.083. This result is in good agreement with previous values of D_1 obtained at comparable Reynolds numbers from wall-heating experiments which used the same boundary layer development area. in the same facility. Both the data and the model, with values of C_1 and C_2 obtained by fitting the model equations to experimental data, show a quadratic-like trend in the level of OPD_{rms} with reduction in wall temperatures, which was also predicted by the full statistical model.

In the regime with the most reduction in wavefront aberrations, $-0.55 < \Delta T/(T_\infty M^2) < -0.35$, there is a corresponding reduction in OPD_{rms} of approximately 75%. The observable scatter in this experimental data in this range is likely due to the fact that in the SBL scaling of the corresponding spectra in this region, the extraction of a small signal from a larger signal can introduce additional uncertainty in the measurement. However, there is strong

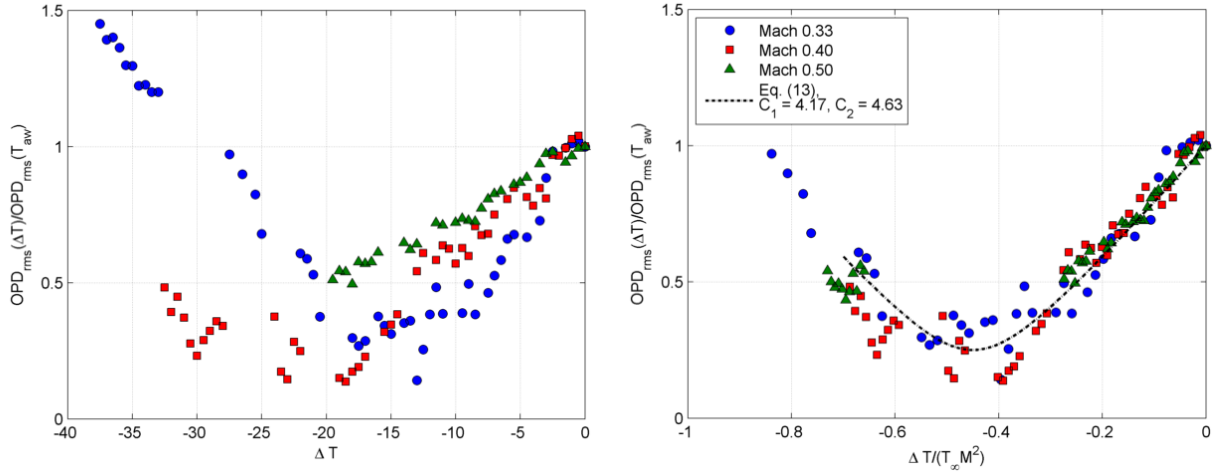

Figure 7. Normalized measurements of $\mathrm{OPD}_{rms}(\Delta T)$ as a function of absolute wall cooling temperature ΔT (left) and the reduced wall temperature for Full wall-cooling case (right).

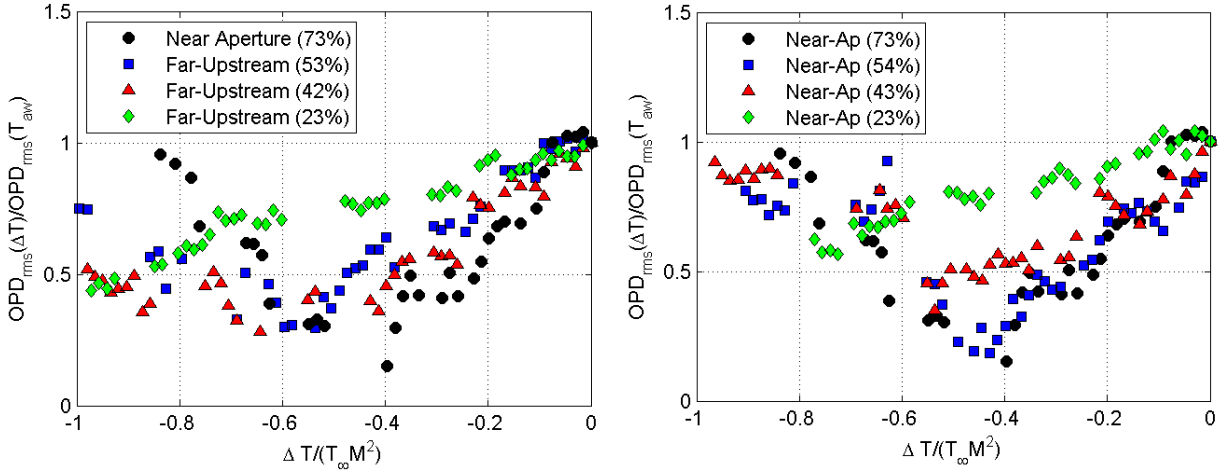

Figure 8. Selected partial wall cooling OPD_{rms} results plotted as a function of $\Delta T/(T_\infty M^2)$ for the near-aperture wall cooling (left), and far-upstream wall cooling cases (right).

qualitative evidence of a significant reduction in levels of aero-optic aberrations around an optimal wall cooling value $\Delta T_{Optimal} \approx -0.45(T_\infty M^2)$ for the 73% near-aperture cooling configuration.

While the empirical values obtained from these cooled-wall wavefront measurements are in good agreement with those obtained for the heated wall over the identical BL development length in [15], neither experiment yields empirical constants which are in agreement with theoretically predicted values of 6.38 and 10.28.. This effect will be discussed in detail later on in this paper.

Experimentally obtained measurements of OPD_{rms} as a function of $\Delta T/(T_\infty M^2)$ are shown in Figure 8 for a number of partial wall-cooling cases. There is a wide range of performance in OPD_{rms} reduction for different cases of partial wall-cooling, in which the location of minimum cooling, and the maximum reduction in OPD_{rms} vary considerably depending on the location and amount of wall cooling. Qualitatively comparing the results for near-aperture wall-cooling in Figure 8, left plot, and far-upstream wall-cooling in Figure 8, right plot, it appears that in general, wavefront measurements with comparable values of R_{cool} result in very similar levels of reduction in OPD_{rms}. For near-aperture cooling $\Delta T_{Optimal}/(T_\infty M^2)$ appears relatively unchanged for different values of $R_{cool} >$ ~40%, while the optimal temperature value is shifting to lower temperatures for the far-upstream cooling results. Values of C_1 and C_2 were estimated for each partial wall-cooling case by fitting equation (18) to the data presented in Figure 8 for each partial wall cooling case. The results are presented in Table 2. From the data presented in Figure 8, the minimum value of OPD_{rms}^{NORM} and the non-dimensional temperature, $\Delta T_{Optimal}/(T_\infty M^2) = -0.5C_1/C_2$, at which OPD_{rms} is minimized at can be estimated. These results are presented for each partial wall cooling case in Table 2, and are also plotted as a function of R_{cool} in Figure 9.

Table 2. Values of C_1, C_2 obtained from SBL wall-cooling wavefront measurements.

Wall Cooling Case	R_{cool}	C_1	C_2	$\frac{\Delta T_{Optimal}}{T_\infty M^2}$	$OPD_{rms}^{NORM}(\Delta T_{Optimal})$
Near-Aperture 1	91.4%	4.80	6.00	-0.40	0.20
Near-Aperture 2	72.6%	4.17	4.63	-0.45	0.25
Near-Aperture 3	22.7%	1.54	1.03	-0.75	0.65
Near-Aperture 4	43.0%	3.33	3.70	-0.45	0.50
Near-Aperture 5	53.9%	4.04	4.49	-0.45	0.30
Far-Upstream 1	23.4%	1.20	0.43	-1.40	0.40
Far-Upstream 2	42.2%	2.14	1.53	-0.70	0.50
Far-Upstream 3	53.1%	2.80	2.33	-0.60	0.40

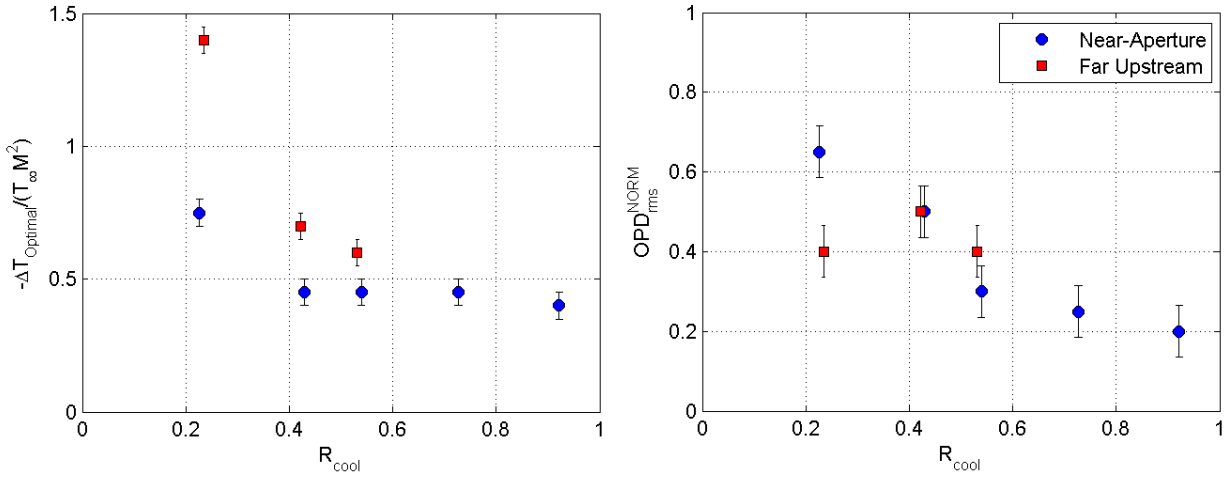

Figure 9. Experimental results for optimal reduced wall cooling temperatures (left) and corresponding levels of optical aberrations (right).

The data presented in Figure 9, right plot, show that in general, cooling a greater percentage of the boundary layer development length upstream of the aperture results in larger reductions in OPD_{rms}. Cooling on ~50% of the turbulent boundary layer development length (either near the aperture or far upstream) is shown to corresponds to a > 60% reduction in OPD_{rms}, while cooling for ~90% of the boundary layer development length results in an 80% reduction in wavefront aberrations. For near-aperture wall cooling, Figure 9, left plot, shows that the location of the optimal temperature does not shift significantly for $R_{cool} > 40\%$, for the near-aperture wall cooling. For far upstream cooling, and partial cooling of both kinds where $R_{cool} < 40\%$, the $\Delta T_{Optimal}$ is shown to decrease. These results demonstrate that partial wall-cooling is can be an effective technique for mitigating TBL wavefront distortions. The near aperture wall cooling was found to be a more efficient method of reducing aero-optical distortions, as the amount of energy, which is proportional to $R_{cool}\Delta T_{Optimal}$, required to attain the maximum reduction in OPD_{rms} is consistently less for near aperture cooling compared to far upstream cooling.

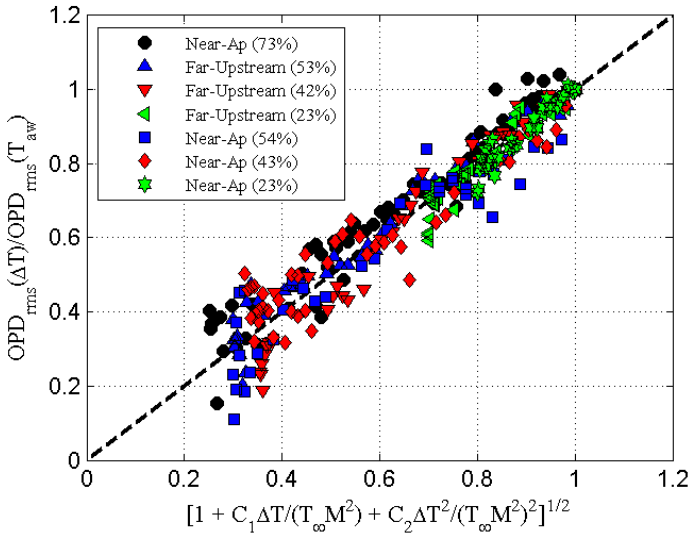

Figure 10. $OPD_{rms}/OPD_{rms}(\Delta T=0)$ plotted versus equation (18) for all tested cooling wall cases.

The comparison between the prediction of the statistical model and experimental measurements of partial wall cooling effects can be seen by plotting OPD_{rms} as a function of equation (18), using the empirical functions C_1 and C_2 obtained for each individual wall-cooling configuration. The results of this comparison are shown in Figure 10, with much of the data lying close to the dashed line of slope 1, indicating a good fit of the experimental data using

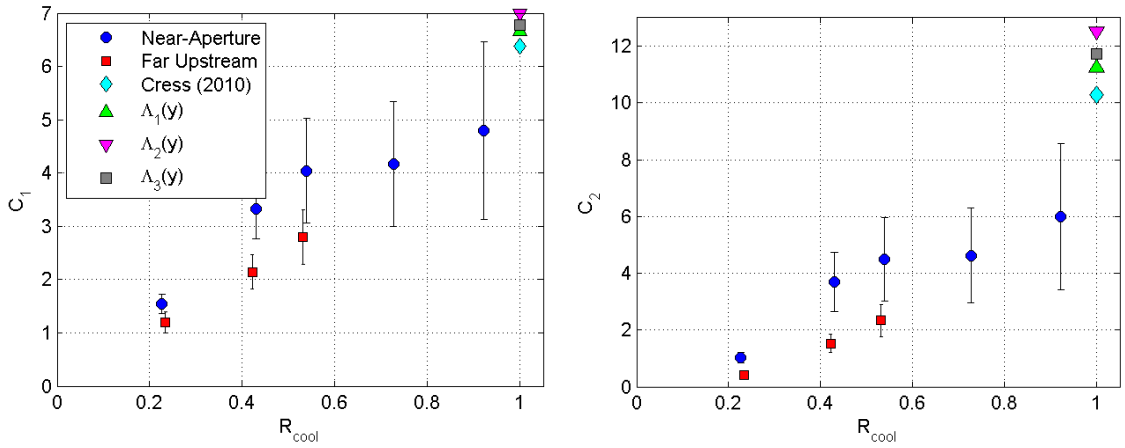

Figure 11. Experimental results for the wall cooling model parameters C_1 (left) and C_2 (right) plotted as a function of R_{cool} for near-aperture and far upstream wall-cooling experimental results compared to values computed from (12b) using different density correlation functions.

the theoretical model for partial wall-cooling over a wide range of partial wall-cooling cases and temperatures. In the region the values for equation (18) are less than 0.4, there is consistently larger scatter of the data about the unity-slope line. This data corresponds to measurements for wall-cooling which resulted reductions in OPD_{rms} greater than 30%, and therefore there is increased experimental uncertainty introduced from SBL scaling.

Figure 11 shows C_1 and C_2 plotted as a function of R_{cool}, for the near aperture and far upstream wall-cooling cases, respectively. Results show that as the area of wall cooling becomes small, C_1 and C_2 also decrease as is expected since in the limit $R_{cool} \rightarrow 0$, it is expected that C_1 and C_2 would also go to zero. Experimentally determined values of C_1 for near aperture and far upstream wall cooling cases are both shown to increase with R_{cool}, but the dependence of C_1 on R_{cool} for these two configurations do not collapse to the same curve. Similar behavior is observed for the C_2. As a limit of the full cooling, both C_1 and C_2, appear to approach values which are somewhat smaller than values computed from (12b) from velocity profiles using several different density correlation functions $\Lambda(y)$ from Figure 1.

The lack of collapse of data for near aperture and far upstream cooling, and the discrepancy with theoretical predictions of constants for the full cooling indicates that partial wall cooling effects on TBL wavefront distortions are not simply a function of the wall area cooled. One possible explanation for the differences in wall-cooling performances for similar values of R_{cool} cooled either near the aperture or far upstream is the relationship between the partial wall cooling wall section and the corresponding thermal sub-layer. A schematic of this is shown in Figure 12, where the top of the thermal sub-layer, δ_0, and the bottom of the sub-layer, δ_1, are approximated using Prandtl's $1/7^{th}$ power law. Then, the ratio of the boundary layer thickness can be expressed as $\delta_{cool}/\delta = (\delta_0 - \delta_1)/\delta$.

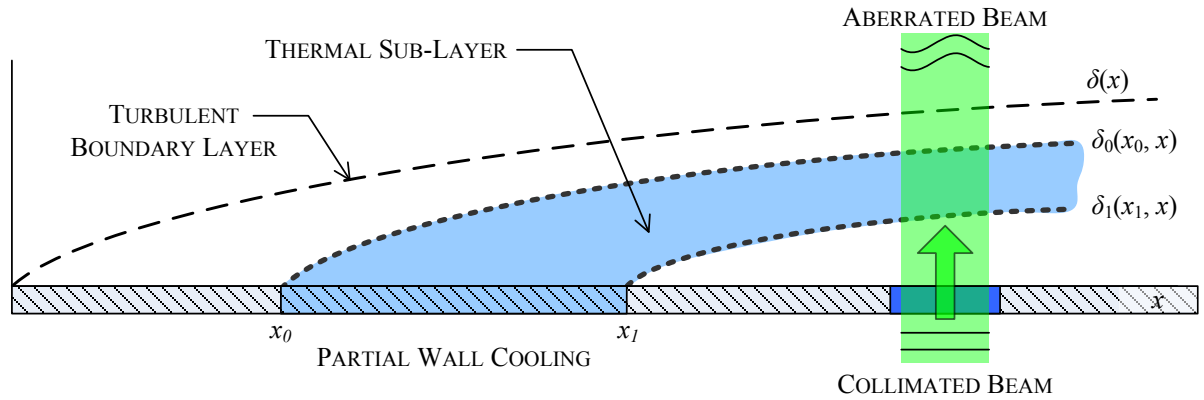

Figure 12. Schematic of thermal sub-layer model of partial wall cooling effects on wavefront aberrations in the TBL.

Although not shown, values of C_1 and C_2 were not found to collapse any better when plotted as a function of δ_{cool}/δ, rather than R_{cool}. This result indicates that the theoretical constants are also not simply a function of the ratio of boundary layer thickness cooled over the optical aperture, but also a function of the region within the TBL which is affected by partial wall cooling at different streamwise locations. To investigate the differences the dependence of C_1 and C_2 on partial wall cooling at different streamwise location, the effect of the thermal sub-layer was modeled by changing the bounds of integration from $y/\delta = [0\ \infty)$ to the thermal sub-layer limits, $[\delta_1\ \delta_0]$ in the theoretical model for the B constants in (12b). Using the results of the modified model (12b), C_1 and C_2 were computed as a function of x_0, x_1 for near aperture and far upstream wall cooling cases. The effect of different density correlation lengths (shown in Figure 13) can also be investigated using this approach. Results of these computations are presented in Figure 13.

Figure 13, top, presents experimental and theoretically predicted values of C_1 using the thermal sub-layer as the bounds of integration for (12b) for different density correlation length functions from Figure 1. The theoretically predicted functions of C_1 using Λ_2 are shown to be qualitatively similar to the trends observed in experimentally measured values of C_1. Similar results are shown for Figure 13, bottom, although theoretically predicted results both constants are consistently larger than the values determined from experimental measurements. This shows that while the inclusion of the thermal sub-layer in the theoretical model does predict the experimentally-observed trends for C-constants for different locations of the wall cooling segment, this simple model still over-predicts the experimentally-measured values for C_1 and C_2 for partial wall cooling effects.

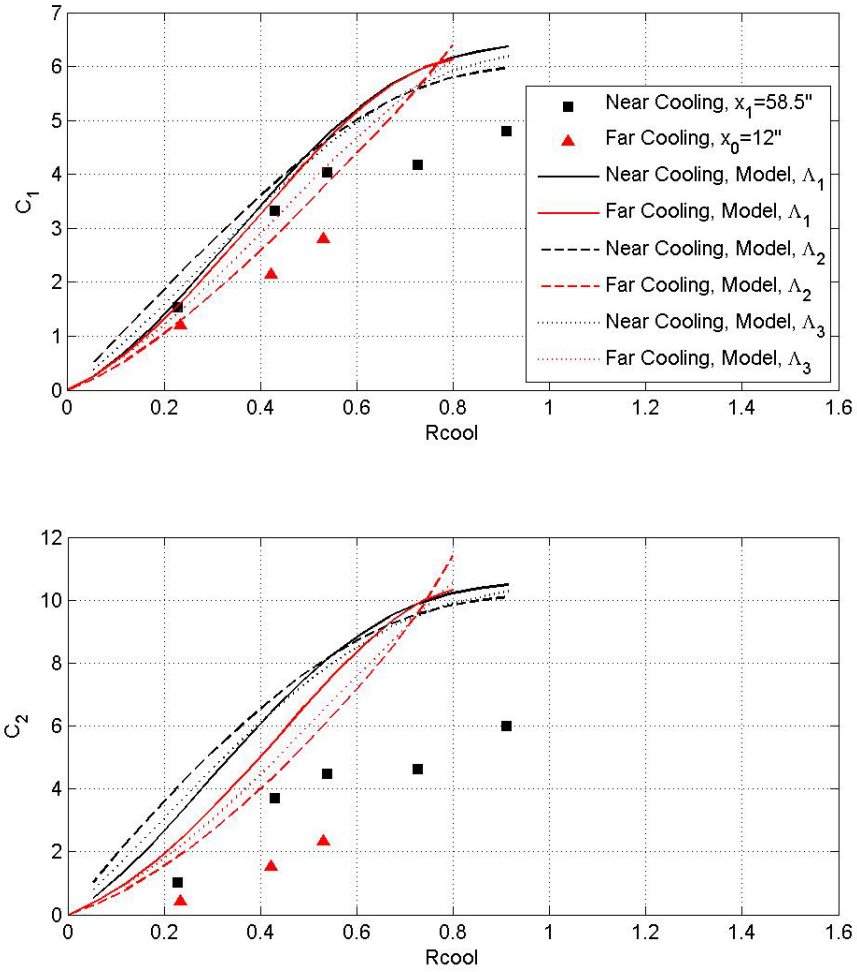

Figure 13. Values of C_1 (top) and C_2 (bottom) calculated for the thermal sub-layer model using equation (12b).

V. Conclusions and Future Work

In this paper, it has been shown from 1-D wavefront measurements of wall-cooling effects on the aero-optics of turbulent boundary layers that the theoretical model proposed by Cress [15], and shown to be valid for experimental measurements of wall-heating in the TBL, is also valid for wall cooling over partial lengths of the boundary layer development section. Comparison of deflection angle spectra for near aperture and far upstream partial wall-cooling cases demonstrated that over a wide range of partial wall configurations and temperatures, the reduction in optical energy is distributed generally evenly over most frequency ranges, with some slight reduction in the effect at high frequencies, $St_\delta > 5$, for shorter lengths of wall cooling. When scaled strictly by a function of wall temperature, deflection angle spectra exhibit self-similarity with baseline wavefront measurements for the adiabatic wall.

Measurements of OPD_{rms} for different partial cooling wall lengths and locations showed that in general, longer wall cooling lengths gave the largest reductions in OPD_{rms} (as high as 80%) at the highest optimal wall-cooling temperature. Although partial wall cooling of about 50% of the boundary layer development length for both cases was shown to result in > 60% reductions in OPD_{rms}, near aperture cooling was shown to consistently have a higher optimal wall-cooling temperature, which corresponds to a smaller amount of energy being extracted from the TBL. This demonstrates that partial wall cooling is an effective method for aero-optic mitigation.

Examining the model parameters C_1 and C_2 calculated for partial wall-cooling, values were shown to monotonically increase with the relative area of wall cooling, R_{cool}, although values for near aperture cooling and far upstream cooling did not appear to exhibit the same dependence on R_{cool}. This indicates that assuming the wall cooling mitigation effect is only proportional to the amount of energy extracted from the flow at a given

temperature, $R_{cool}\Delta T$, is not adequate to describe the behavior of both near aperture and far upstream partial wall cooling. A simple modified theoretical model which accounts for a presence of a finite thermal sub-layer by modifying the bounds of integration on (12b) was introduced. Results of this model, especially those calculated from density correlation length Λ_2, were found to be in good qualitative agreement with experimentally measured trends in C_1 and C_2. However, quantitatively the model over predicts these constants by as much as 40%.

At this point in time, experimental investigations of the effects of partial wall cooling on aero-optic aberrations caused by TBLs has provided valuable preliminary data showing that in general, the statistical model proposed by Cress [15] for wall heating can be extended to wall cooling for full and partial lengths. Partial wall cooling over ~50% of the near aperture length of the boundary layer development section was shown to result in significant reductions in OPD_{rms} on the order of 60%, which is only a 20% loss in performance compared to the 90% wall cooling data obtained.

Also, the results of the partial cooling can be directly applied for the partial heating, as the heating effects are fully described by the constant $D_1 = C_1/2$.

While the theoretical model developed from modifying (12b) to account for the thermal sub-layer shows good qualitative agreement with experimental results obtained so far, the quantitative discrepancy between experimental data and model predictions requires additional analysis of the assumptions involved in the development of the statistical model from [15]. Future work in this area will include a full evaluation of the assumptions of the extended Strong Reynolds Analogy at the root of this statistical model, and the appropriate modifications to the statistical model will be made in order to develop a more robust model for the effects of partial wall-temperature effects.

As part of this work, additional measurements of wavefront aberrations will be made for partial wall cooling and heating on cooled/heated TBLs on both sides of the tunnel walls. This will be done in order to validate the SBL scaling used to extract wall cooling statistics for the double-BL experiment, and to address signal-to-noise errors which result from the use of the SBL scaling technique, especially when aberrations from the cooled-wall boundary layer are significantly smaller than those which result from the un-modified boundary layer. Results from these experiments will be compared to experimental results from the present study, and partial wall-temperature scaling relationships will be refined using DBL, double-wall cooling/heating measurement data as a guide.

Acknowledgments

This work is supported by the Air Force Office of Scientific Research, Grant number FA9550-12-1-0060. The U.S. Government is authorized to reproduce and distribute reprints for governmental purposes notwithstanding any copyright notation thereon.

References

[1] Jumper, E.J., and Fitzgerald, E.J., 2001, "Recent Advances in Aero-Optics," *Progress in Aerospace Sciences,* 37, 299-339.

[2] Wang, M., Mani, A., and Gordeyev, S., "Physics and Computation of Aero-Optics", *Annual Review of Fluid Mechanics*, Vol. 44, pp. 299-321, 2012.

[3] Liepman, H.W., "Deflection and diffusion of a light ray passing through a boundary layer," Report SM-14397. Douglas Aircraft Company, Santa Monica Division, Santa Monica, CA, (1952).

[4] Stine, H.A., and Winovich, W., "Light diffusion through high-speed turbulent boundary layers," Research Memorandum A56B21, NACA, Washington, May 1956.

[5] Sutton, G.W., "Effect of turbulent fluctuations in an optically active fluid medium." *AIAA Journal*, 7(9): 1737-1743, Sept. 1969.

[6] Tatarski, VI, *Wave Propagation in Turbulent Medium*, New York: McGraw-Hill, 1961.

[7] Malley, M., Sutton, G. W. and Kincheloe, N., "Beam-Jitter Measurements of Turbulent Aero-Optical Path Length differences," *Applied Optics*, Vol. 31, pp. 4440-4443 (1992).

[8] Wang, K. and Wang, M., "Aero-optics of subsonic turbulent boundary layers," *Journal of Fluid Mechanics*, Vol. 696, pp. 122-151, 2012.

[9] Wyckham, C., and Smits, A., "Aero-Optic Distortion in Transonic and Hypersonic Turbulent Boundary Layers," *AIAA Journal*, Vol. 47, No. 9, pp. 2158-2168, 2009.

[10] Smith, A.E., Gordeyev, S., and Jumper, E.J., "Recent measurements of aero-optical effects caused by subsonic boundary layers," *Opt. Eng,* 52(7), 071404, 2013.

[11] Gordeyev, S., Jumper, E.J., Ng, T., and Cain, A., "Aero-Optical Characteristics of Compressible, Subsonic Turbulent Boundary Layer," 34th AIAA Plasmadynamics and Lasers Conference, Orlando, Florida, 23-26 June, 2003, AIAA Paper 2003-3606

[12] Wittich, D. J., Gordeyev, S., and Jumper, E. J., "Revised scaling of optical distortions caused by compressible, subsonic turbulent boundary layers." *38th AIAA Plasmadynamics and Lasers Conference*, AIAA-2007-4009, Miami, FL, June 2007.

[13] Cress J., Gordeyev S., Post, M., and Jumper, E.J., "Aero-Optical Measurements in a Turbulent, Subsonic Boundary Layer at Different Elevation Angles," 39th Plasmadynamics and Lasers Conference, Seattle, Washington, 23 - 26 June, 2008, AIAA Paper 2008-4214.

[14] Gordeyev, S., Jumper, E.J., and Hayden, T., "Aero-Optics of Supersonic Boundary Layers," *AIAA Journal*, 50(3), 682-690, 2012. [8]

[15] Cress, J. (2010) *Optical Aberrations Cause by Coherent Structures in a Subsonic, Compressible, Turbulent Boundary Layer,* PhD thesis, University of Notre Dame.

[16] White, M.D., and Visbal, M.R., "Simulation of Aero-Optical interactions in Transonic Boundary Layers," 42nd AIAA Plasmadynamics and Lasers Conference, 27-30 June 2011, Honolulu, Hawaii, AIAA-2011-3279.

[17] White, M.D., and Visbal, M.R., "Aero-optics of compressible Boundary Layers in the Transonic Regime," 43rd AIAA Plasmadynamics and Lasers Conference, 25-28 June 2013, New Orleans, LA, AIAA-2012-2984.

[18] Gordeyev, S., Cress, J., and Jumper, E., "Far-Field Laser Intensity Drop-Outs Caused by Turbulent Boundary Layers", to appear in *Journal of Directed Energy*, 2013.

[19] Smith, A.E., and Gordeyev, S., "Evaluation of Passive Boundary Layer Flow Control Methods for Aero-Optic Mitigation," 51st AIAA Aerospace Sciences Meeting, 6-10 Jan 2013, Grapevine, TX, AIAA Paper 2013-0718.

[20] Gilbert, K.G., "KC-135 Aero-Optical Boundary-Layer/Shear-Layer Experiments," *Aero-Optical Phenomena*, Eds. K.G. Gilbert and L.J. Otten, Vol. 80, *Progress in Astronautics and Aeronautics*, AIAA, New York, 1982, pp. 306-324.

[21] Rose, W.C. and Johnson, E.A., "Unsteady Density and Velocity Measurements in the 6 x 6 ft Wind Tunnel", *Progress in Astronautics and Aeronautics: Aero-Optical Phenomena*, Vol. **80**, edited by K. Gilbert and L.J. Otten, AIAA, New York, pp. 218-232, 1982.

[22] Smith, A.E., Gordeyev, S., and Jumper, E.J., "Aperture Effects on Aero-Optical Distortions Caused by Subsonic Boundary Layers," 43rd AIAA Plasmadynamics and Lasers Conference, 25-28 June 2013, New Orleans, LA, AIAA-2012-2986.